



HAL
open science

Quantifying gene expression domains in plant shoot apical meristems

Pau Formosa-Jordan, Benoit Landrein

► **To cite this version:**

Pau Formosa-Jordan, Benoit Landrein. Quantifying gene expression domains in plant shoot apical meristems. 2022. hal-03909435

HAL Id: hal-03909435

<https://hal.science/hal-03909435v1>

Preprint submitted on 21 Dec 2022

HAL is a multi-disciplinary open access archive for the deposit and dissemination of scientific research documents, whether they are published or not. The documents may come from teaching and research institutions in France or abroad, or from public or private research centers.

L'archive ouverte pluridisciplinaire **HAL**, est destinée au dépôt et à la diffusion de documents scientifiques de niveau recherche, publiés ou non, émanant des établissements d'enseignement et de recherche français ou étrangers, des laboratoires publics ou privés.



Distributed under a Creative Commons Attribution 4.0 International License

Quantifying gene expression domains in plant shoot apical meristems

Pau Formosa-Jordan^{1,2}, Benoit Landrein^{1,3}.

1. Sainsbury Laboratory, University of Cambridge, Cambridge, United Kingdom.
2. Department of Plant Developmental Biology, Max Planck Institute for Plant Breeding Research, Cologne, Germany.
3. Laboratoire Reproduction et Développement des Plantes, Univ. Lyon, ENS de Lyon, UCB Lyon 1, CNRS, INRAE, INRIA, 69364 Lyon Cedex 07, France.

Correspondence: pformosa@mpipz.mpg.de

i. Running Head: Quantifying expression domains in shoot meristems

ii. Abstract

The shoot apical meristem is the plant tissue that produces the plant aerial organs such as flowers and leaves. To better understand how does the shoot apical meristem develop and adapt to the environment, imaging developing shoot meristems expressing fluorescence reporters through laser confocal microscopy is becoming increasingly important. Yet, there are not many computational pipelines enabling a systematic and high-throughput characterisation of the produced microscopy images. This chapter provides a simple method to analyse 3D images obtained through laser scanning microscopy and quantitatively characterise radially or axially symmetric 3D fluorescence domains expressed in a tissue or organ by a reporter. Then, it presents different computational pipelines aiming at performing high-throughput quantitative image analysis of gene expression in plant inflorescence and floral meristems. This methodology has notably enabled to characterise quantitatively how stem cells responded to environmental perturbations in the *Arabidopsis* inflorescence meristem and will open new avenues in the use of quantitative analysis of gene expression in shoot apical meristems. Overall, the presented methodology provides a simple framework to analyse quantitatively gene expression domains from 3D confocal images at the tissue and organ level, which can be applied to shoot meristems and other organs and tissues.

iii. Keywords: quantitative image analysis, confocal microscopy, expression domain, floral meristem, inflorescence meristem, stem cells, *Arabidopsis*.

1. Introduction

Plant morphogenesis mainly relies on the maintenance of post-embryonic stem cells activities located in specific regions referred as meristems. The maintenance of the pool of stem cells in the *Arabidopsis* shoot apical meristem (SAM) largely depends on a feedback loop between *WUSCHEL* (*WUS*), a mobile homeodomain transcription factor promoting stem cell proliferation, and *CLAVATA3* (*CLV3*), a diffusing peptide whose expression is induced by *WUS* but which restricts its expression through binding to specific receptors [1–5]. The dynamic expression of *WUS* and *CLV3* in specific domains, the organising centre and the central zone respectively, are key for orchestrating stem cell homeostasis. Furthermore, stem cell homeostasis has been shown to depend on additional regulators such as cytokinins and transcription factors from the HAIRY MERISTEM (HAM) family, whose expression in the SAM is also tightly regulated [6–9].

Studying the spatiotemporal dynamics of the stem cell regulatory network is primordial to understand its function. In the recent years, live imaging techniques relying on the use of fluorescent reporters imaged by 3D laser scanning microscopy have been developed, allowing time-lapse imaging of gene expression in both inflorescence and floral meristems [10, 11]. Having a quantitative analysis of such expression domains is pivotal for a better understanding of stem cell behaviour, and has notably been used to evaluate stem cell plasticity and robustness upon environmental perturbations [12]. As these expression domains span over dozens or hundreds of cells, it is convenient to have pipelines optimised to extract certain quantities at the tissue level (see **Note 1**).

This chapter presents a simple method that enables a high-throughput extraction and quantification of either radially or axially symmetric expression domains in the shoot

meristems from 3D laser scanning microscopy images. Taking advantage of the symmetry of the expression domains, the method that is proposed extracts the fluorescent signal of the domain but also a characteristic length of the domain – a proxy of the size of the studied domain – by fitting a function to a radial fluorescence profile. The size of the expression domains of key regulators acting in the plant shoot meristems has been shown to be very relevant for understanding how the plant develops and adapts to environmental cues [8, 12], and therefore, it is paramount to develop methods that facilitate its quantification. The presented method also provides, along with other features, the mean autofluorescence levels surrounding the expression domain, which facilitates the extraction of the fluorescence levels in the expression domains, as well as a radial profile shape.

Along with the presentation of the method in detail, this book chapter further outlines two main applications to characterise fluorescence domains in inflorescence and floral meristems in a high-throughput manner. These pipelines include pre-processing steps, domain detection and analysis using the proposed fluorescence profile fitting method. Overall, this chapter provides the reader with different tools to quantitatively characterise fluorescence domains in the shoot meristems. This chapter will not address aspects in relation to live imaging of the shoot meristems, and we recommend the reader to refer to other sources for this purpose (*e.g. see [10, 12]*).

2. Method

2.1 Characterisation of a fluorescence domain

This method consists on extracting, from a 3D confocal microscopy stack, basic measurements of a fluorescence domain whose z-projection is radially symmetric (*see Note 2*) and exhibits higher fluorescence levels at the centre of the domain.

Specifically, this method takes advantage of the radially symmetric decay of the fluorescence in the expression domain to compute a characteristic length L , which can be used as a proxy of the expression domain size.

To extract the radial fluorescence profile, the method performs an angular integration around the centroid of the fluorescence domain on the sum slices projected and Gaussian blurred image (Fig. 1). The angular integration consists in computing the mean fluorescence intensity of N concentric subregions within a circular region R around the centroid \mathbf{r}_0 . The most central subregion is a circle of a certain radius $d\rho$, and the other subregions are $N-1$ concentric i-rings ($i=1, \dots, N-1$) of width $d\rho$ filling the R region (Fig. 1B); the i -th ring is defined by those pixels whose (x,y) coordinates fulfil the relation $\rho_i^2 < (x-x_0)^2 + (y-y_0)^2 \leq \rho_{i+1}^2$, x_0 and y_0 being the coordinates of the centroid \mathbf{r}_0 and where $\rho_i = i d\rho$.

Then, the fluorescence profile can be fitted to several possible functions, such that we can extract the domain features more straightforwardly. In particular, we fit the profile to a generalised exponential function [13] defined as

$$F_E(r) = C_E + D_E e^{-\left(\frac{r}{L_E}\right)^{n_E}}, \quad (1)$$

and to a decreasing Hill function of the form

$$F_H(r) = C_H + \frac{D_H}{1 + \left(\frac{r}{L_H}\right)^{n_H}}, \quad (2)$$

L_X being the characteristic length of the domain [13], C_X the mean autofluorescence levels of the sum slices projection, D_X the height of the fluorescent peak or mean maximal levels, and n_X an exponent accounting for the radial decay of the fluorescent domain, what we will refer as profile shape parameter; X denotes the use of either the generalised exponential ($X=E$) or the Hill ($X=H$) fitting function. Note that apart from L_X , the fit also determines the parameters C_X , D_X and n_X , defined above (Fig. 1C).

We expect that certain profiles will fit better to a Hill profile, *e.g.*, in the case of a profile presenting a sigmoidal shape, while other profiles having a smoother decay will have a better fit to a generalised exponential function (we discuss how to determine the best fit in the inflorescence pipeline subsection). From Eqs. (1) and (2) we can see that L_E and L_H provide the distance from the centre of the fluorescence domain at which the maxima intensity decreases ‘e’-fold and 2-fold, respectively (Fig. 1C), having subtracted the autofluorescence. Hence, unless the fluorescence domain boundary is very well defined by a sharp decline of the fluorescence intensity, such characteristic lengths L_E and L_H should not be interpreted as an exact radius of the whole fluorescence domain, but rather as a characteristic size associated to it. Note that the concept of a characteristic size has been widely used for characterising morphogen gradients [13–15]. The shape parameter of the generalised exponential fit, n_E , will tell us whether the profile is wider ($n_E < 2$) or narrower ($n_E > 2$) than a Gaussian, while the shape parameter from the Hill fit, n_H , will give an idea of how sigmoidal the profile is, by how large n_H will be. The mean maximal levels D_X might also be informative and show interesting behaviours upon certain perturbations. Apart from these signal profile features, one may want to find the total fluorescence in the defined region R of the studied domain, what we refer as M_R . The fitting function method also helps in this purpose, as it infers the mean autofluorescence C_X , which needs to be properly subtracted from the total fluorescence.

To compute the total fluorescence of the selected domain, we perform the following operation:

$$M_R = \gamma \sum_{i \in R} p_i , \quad (3)$$

where p_i are the pixel intensity levels in the i -th pixel of the sum slices projection, and γ is the resolution in square microns units of the z-projected image under study. The γ

factor corrects the differences in intensity levels between images that have different resolution in the xy plane (*see Note 3*).

Then, the total autofluorescence in the R region, derived by the Hill or generalised exponential fitting, denoted by $B_{R,X}$, is subtracted from the summed fluorescence in the selected domain, namely,

$$I_{R,X} = M_R - B_{R,X} , \quad (4)$$

where $B_{R,X}=C_X A_R$, being A_R the area of the R region.

Below, we provide applications of the presented method through different pipelines applied to analyse expression domains in *Arabidopsis* inflorescence and floral meristems. These applications can be straightforwardly adapted to study any 3D fluorescence profile whose 2D projection is radially symmetric.

2.2 Applications

The reader can put into practice the presented method through pipelines that have been implemented with the Matlab RegionsAnalysis code (<https://gitlab.com/sluc/teamHJ/pau/RegionsAnalysis>, *see Notes 4 and 5*). The relevant pipelines can be executed by means of the different scripts located in the RegionsAnalysis/Applications/ShootMeristemsAnalysis subfolder, with the help of the *Readme* file found in the same folder. Such pipelines will enable to analyse at once all the multichannel microscopy z-stacks in either *lsm* or *dzi* formats that are located in a specific folder. After executing the pipelines of interest, different outputs will be generated in the containing folder of the microscopy data, including a *csv* file with the main descriptors of the studied fluorescence domains (*see Readme* file). Available microscopy data of shoot meristems with fluorescence reporters can be found at [16].

As a start, we suggest the reader to use the script *main_script_basicpipeline_fittings*, which enables the user to define the fluorescence domains under study by manually selecting the different domains of interest (see *Readme* file). This script will compute the characteristic sizes and fluorescence intensities of the selected domains. The reader can use this script to have a sense of how large the *R* regions surrounding the fluorescence domains should be, and it can be useful to get familiarised with other parameters that will be used in the other pipelines as well (see **Note 6**).

The two other pipelines presented below automatically find the expression domains of interest in the *z*-stack, the first pipeline focusing on analysing gene expression in the inflorescence meristem and the second one in floral meristems. Domain extraction is performed on a Gaussian filtered maximal intensity slices projection of the fluorescence image under study, while the analysis of the domains (*e.g.*, the size computation) is performed on a Gaussian filtered sum slices projection (Fig. 2). In both tasks, the Gaussian filter is used to smooth out the fluorescence images and get rid of local variations in signal due to the intracellular localisation (either nuclear or endoplasmic reticulum) of the fluorescent markers (see **Note 7**). The automatic identification of the expression domains is performed through an Otsu thresholding over the corresponding *z*-projected and Gaussian filtered fluorescence images [17] (see **Note 8**). These pipelines assume that the images are acquired such that the *z*-stacks show transversal sections of the meristems. Note that to correctly detect the inflorescence and floral fluorescence domains, the inflorescence meristem should be as close as possible to the centre of the image.

2.2.1 Inflorescence Meristem Pipeline

This pipeline can be executed by running the script

main_script_inflorescence_meristem, which consists of the following main stages

(Fig. 2):

1.- Automatic detection of the expression domain in the inflorescence meristem. This pipeline executes some pre-processing steps as mentioned above, followed by an Otsu thresholding, producing a binarised image, with domains having a value of 1 when the pixel intensity is above the threshold, and 0 when it is below. As the floral primordia usually also express the reporters present in the inflorescence meristem, the binarised image shows multiple domains. Then, the code assumes that the binarised domain corresponding to the inflorescence meristem is the one that is the closest to the geometric centre of the ensemble of the domains' centroids in each image (*see Note 9*). Then, the code finds the centroid of the inflorescence domain, r_0 , and defines a circular region R of radius ρ_R that should contain the fluorescence domain under study in the meristem. It is important to manually check whether the automatic detection of the domain at the inflorescence meristem has been correctly performed (*see Notes 9, 10 and 11*).

2.- Intensity profile extraction, intensity profile fitting and features extraction. As explained above, after extracting the mean radial intensity profile, the code fits it to two different functions (Eqs. 1 and 2). Then, one can visually assess which fit is better [18], and complement it with different measurements and/or statistical indicators the reader find useful (*see Note 12*). In the studied case shown in Fig. 3 of the domain of expression of a *pWUS::GFP-ER* reporter, we find that Hill fittings tend to underestimate the autofluorescence levels (Fig. 3C, *see Note 13*), leading for instance to negative values of the mean autofluorescence; the exponential fittings tend to be

better for such kind of expression domain. Note though, that the characteristic length would be proportionally similar in both Hill and generalised exponential descriptions (Fig. 3B) (*see Note 14*).

Overall, this pipeline enables to quantitatively characterise in a high-throughput manner the features of fluorescence domains in the inflorescence meristem.

Importantly, this pipeline can be used to determine whether different growth conditions or treatments have an effect into the fluorescence domains of the inflorescence meristem (Fig. 3). To determine the statistical significance of the effect, the reader will have to complement this analysis with the appropriate statistical tests [*12, 19*]. As we previously reported, we applied this pipeline to study the effect of mineral nutrition on the expression of *WUS* in the *Arabidopsis* inflorescence meristem [*12*]. As shown in Fig. 3D and E, this quantification allowed us to show a very strong correlation between the expression of a *pWUS::GFP-ER* reporter (both in terms of signal intensity and domain size) with the size of the inflorescence meristem and with the amount of nutrients with which the plant was grown [*12*].

2.2.2 Floral meristems pipeline

This pipeline can be executed by running the script *main_script_floral_meristems*, which consists of the following stages (Fig. 4):

- 1.- Manual outlining of the different floral meristems in a Gaussian blurred sum slices projection of the autofluorescence channel image or a fluorescence channel image that shows the floral meristems (*see Notes 15 and 16*). In a later stage of the pipeline, such primordia outlines will be paired with automatically found fluorescence domains, and the domains remaining unpaired with outlined primordia will be

discarded. Hence, this first stage will help determining the floral fluorescence expression domains of interest. This stage also allows to compute the projected area of the floral primordia and their distance from the centre of the inflorescence meristem (*see Note 17*).

2.- Automatic detection of the floral fluorescence domains. As in the inflorescence meristems pipeline, some pre-processing steps are executed, followed by an Otsu thresholding. In order to detect weaker fluorescence domains, the Otsu threshold can be reduced by a certain factor (*see Notes 8 and 18*). In this pipeline, the inflorescence domain, detected as explained in the previous pipeline, is the one that is discarded for the analysis. Then, the code outlines the different R regions centred around the automatically detected floral expression domains. Such regions will vary in size such that the profile fittings can be better performed (*see Note 19*).

3.- Intensity profile extraction, intensity profile fitting and features extraction. As in the pipeline for the inflorescence meristems, one needs to find out which kind of fitting works better for the posterior feature extraction. We found that the floral *pWUS::GFP-ER* intensity profile had a better match with the generalised exponential fit, as it was the case for the inflorescence domain.

4.- Pairing of the outlined floral meristems and the automatically found fluorescence expression domains. The automatically found domains that could not be paired with the manually outlined primordia are discarded. This pairing step usually helps in discarding the fluorescence domains that do not belong to the studied floral primordia (for instance, when only floral primordia of a certain stage are considered), and hence, it can be used as a validation step of the found domains.

As a proof of principle, we have applied this pipeline to compute the radial distance between the primordia and the centre of the inflorescence meristem, a parameter that

correlates with the size of the primordia (Fig. 5A) and can be used to order these primordia by age [20–22]. This pipeline can also reveal interesting correlations such as the expected one we observed between the expression of the *pWUS::GFP-ER* reporter and the age of the primordia (defined through their radial distance from the centre of the inflorescence meristem Fig. 5B) [8]. This pipelines can be easily extended to characterise other relevant morphogenic quantities like the plastochron ratio [22], and the phyllotactic pattern.

Overall, this pipeline enables a high-throughput characterisation of the floral expression domains, which, together with the inflorescence expression domains, still remains highly unexplored.

3. Notes

1. Studies in the shoot tissues at the single cell resolution are pivotal for understanding different morphogenetic processes [23], but can also be very labour intensive; such studies often require the imaging of additional dyes or fluorescence reporters to enable cell or nuclear segmentation with rather computationally intensive algorithms [24–31]. For simplicity, this chapter only focuses on tissue-level characterisation of fluorescence domains.
2. We refer here to z-projections, assuming that the radial symmetry of the fluorescence domain is shown the xy plane. If the radial symmetry is observed in xz or yz planes, the image can be simply properly rotated to get the symmetry in the xy plane, or the pipeline can be adapted.
3. For simplicity, we assume that different images of an experimental set have the same resolution in the z direction. If it is not the case, the γ factor needs to be the

resolution of the 3D image (in μm^3) to also take into account different resolutions in the z direction.

4. The experienced Matlab coder is encouraged to extract further observables from the fluorescence domains. See *Readme* file of the described pipelines in the RegionsAnalysis code. Also, we encourage the reader to push such code changes back to the RegionsAnalysis repository in GitLab, so that others can benefit from them.

5. It has been shown that the stem-cell niche can scale with the size of the inflorescence meristem [8, 12]. Hence, it can be interesting to combine the current method and pipelines with morphological analyses of the meristem (see for instance tools for 3D morphological analyses in SAMs provided in [26, 32]), to evaluate possible correlations between fluorescence domains and shoot meristem morphology.

6. We also provide the script *main_script_ROIs*, which can be used as a basic Region of Interest (ROI) manager to compute mean fluorescence intensities of regions of interest (see *Readme* file), and, for instance, can help in manually corroborating the autofluorescence levels.

7. By default, we use a 2-D Gaussian blur with a smoothing kernel with standard deviation of $\sigma=5\mu\text{m}$.

8. The Otsu thresholding method automatically finds an optimal threshold to the studied image by maximising a measure of ‘separability’ in the grayscale image histogram, based on the first statistical cumulative moments [17]. Given that the fluorescence domains can be smooth and with different intensities, the Otsu threshold level might not optimally separate the background from the fluorescence domains. For this reason, we have included the Otsu prefactor, which can help to better detect all the domains of interest.

9. To find the fluorescence domain of the inflorescence meristem, depending on the images and the fluorescence reporters under study, the Otsu prefactor may need to be adjusted. Also, the algorithm itself can be easily changed to find the fluorescence domain of the inflorescence meristem (*e.g.*, in some cases, finding the largest fluorescence domain may be a good alternative). If that domain is not properly found in an automatic manner, note the pipeline can be run by doing the manual selection of the fluorescence domain under study (see *Readme* file).

10. By default, the radius of the region R for the inflorescence domain under study is set to $\rho_R=40\ \mu\text{m}$, and $d\rho=1\ \mu\text{m}$ (leading to $(N-1)=39$ concentric rings). Choosing an optimal radius of region R (ρ_R) containing the inflorescence domain is pivotal; a too small ρ_R will make more difficult the inference of the mean autofluorescence, while a too large ρ_R might drive the inadequate inclusion of other fluorescence domains in the same R region, distorting the extraction of the fluorescence profile for the inflorescence domain. See **Note 19** for the determination of R in floral domains.

11. This pipeline can also produce projections of the xz and yz ortho-slices, providing further information on the 3D morphology of the fluorescence domain under study.

12. Note that the R-square coefficient of the nonlinear fit will not be a very good indicator for our purpose [33], although we provide it as an outcome in the pipeline; usually, the discrepancies of the fit with the data will be more in the fluorescence decay tail and in the fluorescence maxima, and this may be difficult to grasp with this coefficient.

13. We invite the reader to also compute the autofluorescence mean levels through an alternative method, *e.g.* by measuring it with Fiji [34], or by executing the script *main_script_ROIs* from RegionAnalysis.

14. When fittings are showing a low degree of variability on the profile shape parameters n_X , one can find the average of these parameters and perform again the fittings, but having the exponents fixed by these averages.
15. To outline the floral primordia, the sum slices projection of the autofluorescence image (*i.e.*, image channel intended to capture the red/far red autofluorescence of the chlorophyll) provides a clearer picture than the maximal slices projection. Outlining the floral primordia might also be possible in the sum slice projection of the fluorescence reporter under study. Note that visualising the slice projection in the fire colour code facilitates the outlining of the primordia.
16. After outlining each primordium, one can assign a number to it. If the reader is interested in the phyllotactic pattern, it might be useful to assign the order of appearance of the primordia, as shown in Fig. 4.
17. Omitting the manual outlining stage may be possible if the detection of the domains is good enough, and if the floral primordia projected areas are not of interest. If this stage is omitted, the pairing stage will not be necessary.
18. To detect a maximal number of floral expression domains, the Otsu prefactor might need to be further adjusted; the prefactor might need to be smaller than 1 to detect weakly fluorescent floral domains, but large enough such that neighbouring expression domains are not merged when thresholding is performed. Note that domain fusion might disrupt the detection of the inflorescence meristem. By default, we set the Otsu prefactor to 0.7.
19. To extract the intensity profiles of the different floral domains, note that one needs to optimise the sizes of the R domains and minimise overlaps between R domains, such that an R domain just contains one floral domain. In order to do that, the R domain size will be proportional in size to the mask of the domain after thresholding.

Furthermore, we need to ensure a minimal size of the domain such that the profile fitting can have a good estimation of the autofluorescence. See corresponding *Readme* file in the GitLab repository for further details.

Acknowledgements

BL and PFJ thank James Locke, Elliot Meyerowitz and Henrik Jönsson for fruitful discussions and their support. PFJ would like to thank Michael Elowitz and Pulin Li for discussions about the quantification of fluorescence domains that had an influence on the elaboration of the presented method, Hugo Tavares for feedback on the data analysis. PFJ also thanks George Coupland and Martina Cerise for fruitful discussions and Gabriel Rodriguez Maroto and Pau Casanova-Ferrer for a critical feedback on the manuscript and for having contributed to the current version of the RegionsAnalysis code; the pipelines they have contributed to will be discussed elsewhere. PFJ is grateful to the Herchel Smith Foundation for funding his postdoctoral fellowship. PFJ and BL thank the Gatsby Charitable Foundation for the provided support and PFJ thanks the Max Planck Society for its support as well.

References

1. Schoof H, Lenhard M, Haecker A, et al (2000) The stem cell population of Arabidopsis shoot meristems is maintained by a regulatory loop between the CLAVATA and WUSCHEL genes. *Cell* 100:635–644.
2. Fletcher JC, Brand U, Hobe M, et al (2000) Stem cell fate in Arabidopsis thaliana depends on a feedback loop regulated by CLV3 activity. *Mol Biol Cell* 11:1497
3. Yadav RK, Perales M, Gruel J, et al (2011) WUSCHEL protein movement mediates stem cell homeostasis in the Arabidopsis shoot apex. *Genes Dev* 25:2025–2030. doi:10.1101/gad.17258511
4. Daum G, Medzihradzky A, Suzuki T, Lohmann JU (2014) A mechanistic framework for noncell autonomous stem cell induction in *Arabidopsis*. *Proc Natl Acad Sci U S A* 111:14619–14624. doi:10.1073/pnas.1406446111
5. Lopes FL, Galvan-Ampudia C, Landrein B (2021) WUSCHEL in the shoot apical meristem: old player, new tricks. *J Exp Bot* 72:1527–1535. doi:10.1093/jxb/eraa572

6. Zhou Y, Liu X, Engstrom EM, et al (2015) Control of plant stem cell function by conserved interacting transcriptional regulators. *Nature* 517:377–380. doi:10.1038/nature13853
7. Zhou Y, Yan A, Han H, et al (2018) Hairy meristem with wuschel confines *clavata3* expression to the outer apical meristem layers. *Science* 361:502–506. doi:10.1126/science.aar8638
8. Gruel J, Landrein B, Tarr P, et al (2016) An epidermis-driven mechanism positions and scales stem cell niches in plants. *Sci Adv* 2:e1500989–e1500989. doi:10.1126/sciadv.1500989
9. Gruel J, Deichmann J, Landrein B, et al (2018) The interaction of transcription factors controls the spatial layout of plant aerial stem cell niches. *npj Syst Biol Appl* 4:36. doi:10.1038/s41540-018-0072-1
10. Heisler MG, Ohno C (2014) Live-Imaging of the Arabidopsis Inflorescence Meristem. In: Riechmann JL, Wellmer F (eds) *Flower Development. Methods and Protocols. Methods Mol Biol*, vol 1110. Humana Press, New York, NY. doi.org:10.1007/978-1-4614-9408-9_25.
11. Prunet N, Jack TP, Meyerowitz EM (2016) Live confocal imaging of Arabidopsis flower buds. *Dev Biol* 419:114–120. doi:10.1016/j.ydbio.2016.03.018
12. Landrein B, Formosa-Jordan P, Malivert A, et al (2018) Nitrate modulates stem cell dynamics in Arabidopsis shoot meristems through cytokinins. *Proc Natl Acad Sci U S A* 115:1382–1387. doi:10.1073/pnas.1718670115
13. Bergmann S, Sandler O, Sberro H, et al (2007) Pre-steady-state decoding of the bicoid morphogen gradient. *PLoS Biol* 5:0232–0242. doi:10.1371/journal.pbio.0050046
14. Ibañes M, Belmonte JCI (2008) Theoretical and experimental approaches to understand morphogen gradients. *Mol Syst Biol* 4:176. doi:10.1038/msb.2008.14
15. Li P, Markson JS, Wang S, et al (2018) Morphogen gradient reconstitution reveals Hedgehog pathway design principles. *Science* 360:543–548. doi:10.1126/science.aao0645
16. Landrein B, Formosa-Jordan P, Malivert A, et al (2018) Research data supporting “Nitrate modulates stem cell dynamics in Arabidopsis shoot meristems through cytokinins” [Dataset]. doi:10.17863/CAM.18621.
17. Otsu N (1979) A Threshold Selection Method from Gray-Level Histograms. *IEEE Trans Syst Man Cybern* 9:62–66. doi:10.1109/TSMC.1979.4310076
18. Motulsky HJ, Ransnas LA (1987) Fitting curves to data using nonlinear regression: a practical and nonmathematical review. *FASEB J* 1:365–374. doi:10.1177/0032329209357884
19. John H McDonald (2014) *Handbook of Biological Statistics, Third Edit.* Sparky House Publishing, Baltimore, Maryland, U.S.A
20. Richards FJ (1951) Phyllotaxis: Its Quantitative Expression And Relation To Growth In The Apex. *Philos Trans R Soc London* 235:509–564
21. Erickson RO., Meicenheimer RD (1977) Photoperiod Induced Change in Phyllotaxis in *Xanthium*. *Amer J Bot* 64:981–988
22. Landrein B, Refahi Y, Besnard F, et al (2015) Meristem size contributes to the robustness of phyllotaxis in Arabidopsis. *J Exp Bot* 66:1317–1324. doi:10.1093/jxb/eru482
23. Formosa-Jordan P, Teles J, Jönsson H (2018) Single-Cell Approaches for Understanding Morphogenesis Using Computational Morphodynamics. In:

- Morris R (ed) *Mathematical modelling in plant biology*. Springer, Cham.
24. Barbier de Reuille P, Routier-Kierzkowska A-L, Kierzkowski D, et al (2015) MorphoGraphX: A platform for quantifying morphogenesis in 4D. *Elife* 4: e05864. doi:10.7554/eLife.05864
 25. Willis L, Refahi Y, Wightman R, et al (2016) Cell size and growth regulation in the *Arabidopsis thaliana* apical stem cell niche. *Proc Natl Acad Sci U S A* 113:E8238–E8246. doi:10.1073/pnas.1616768113
 26. Kiss A, Moreau T, Mirabet V, et al (2017) Segmentation of 3D images of plant tissues at multiple scales using the level set method. *Plant Methods* 13:114. doi:10.1186/s13007-017-0264-5
 27. Montenegro-Johnson T, Strauss S, Jackson MDB, et al (2019) 3DCellAtlas Meristem: A tool for the global cellular annotation of shoot apical meristems. *Plant Methods* 15:33. doi:10.1186/s13007-019-0413-0
 28. Bhatia N, Åhl H, Jönsson H, Heisler MG (2019) Quantitative analysis of auxin sensing in leaf primordia argues against proposed role in regulating leaf dorsoventrality. *Elife* 8:e39298. doi:10.7554/elife.39298
 29. Meyer HM, Teles J, Formosa-Jordan P, et al (2017) Fluctuations of the transcription factor ATML1 generate the pattern of giant cells in the *arabidopsis* sepal. *Elife* 6:e19131. doi:10.7554/eLife.19131.001
 30. Fernandez R, Das P, Mirabet V, et al (2010) Imaging plant growth in 4D: robust tissue reconstruction and lineaging at cell resolution. *Nat Methods* 7:547. doi:10.1038/nMeth.1472
 31. Wolny A, Cerrone L, Vijayan A, et al (2020) Accurate and versatile 3D segmentation of plant tissues at cellular resolution. *Elife* 9:e57613. doi:10.7554/elife.57613
 32. Åhl H, Zhang Y, Jönsson H (2022) High-Throughput 3D Phenotyping of Plant Shoot Apical Meristems From Tissue-Resolution Data. *Front Plant Sci* 13: 827147. doi:10.3389/fpls.2022.827147
 33. Spiess AN, Neumeyer N (2010) An evaluation of R2 as an inadequate measure for nonlinear models in pharmacological and biochemical research: A Monte Carlo approach. *BMC Pharmacol* 10:6. doi:10.1186/1471-2210-10-6
 34. Schindelin J, Arganda-Carreras I, Frise E, et al (2012) Fiji: an open-source platform for biological-image analysis. *Nat Methods* 9:676–82. doi:10.1038/nmeth.2019

Figures

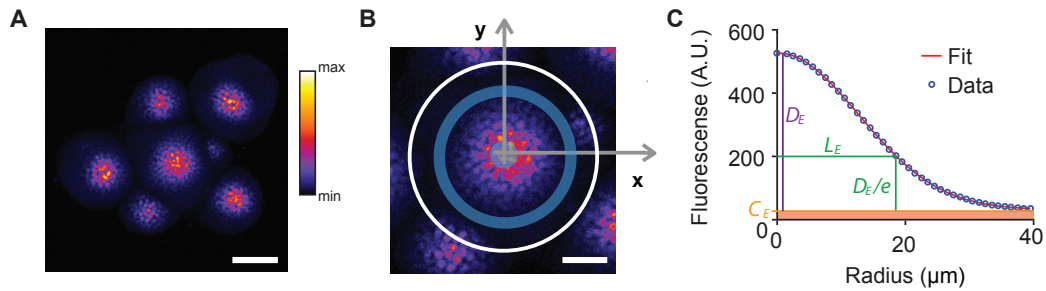


Figure 1.- Method for fluorescence domain characterisation. (A) Maximal intensity projection of a 3D confocal microscopy stack of the shoot apical meristem, showing the *pWUS::WUS-GFP* expression pattern. (B) Illustrating the profile extraction in a zoomed image of the inflorescence domain shown in A. The outer white circle denotes the limits of the R region of interest (ROI) where the radial intensity profile will be computed. Within this region, the average intensity is computed within concentric rings like the blue one depicted. The blue circle at the centre illustrates the discrete unit for computing the average intensity at the origin of the intensity profile. (C) Radial intensity profile with a generalised exponential fit. The fit allows to extract the characteristic size L_E at which the maximal signal D_E has dropped an e -factor, having subtracted the inferred mean autofluorescence C_E . Our method proposes the extraction of this characteristic size as a proxy of the fluorescence domain size. Scale bars: $50 \mu\text{m}$ (A), $25 \mu\text{m}$ (B). Panels modified from [12].

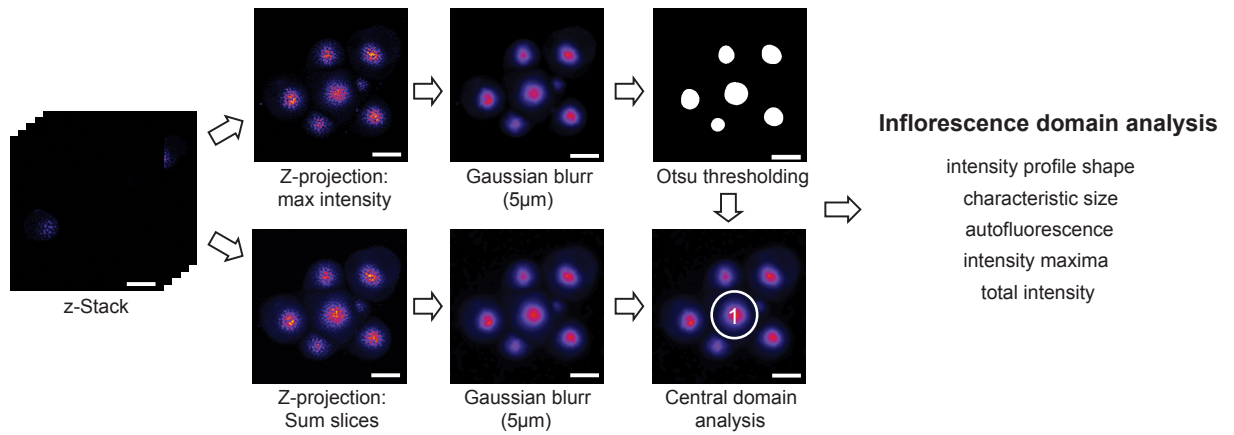


Figure 2.- Sketch of the inflorescence meristems pipeline on images showing the *pWUS::WUS-GFP* reporter. Adapted from [12]. Scale bars: 50 μm .

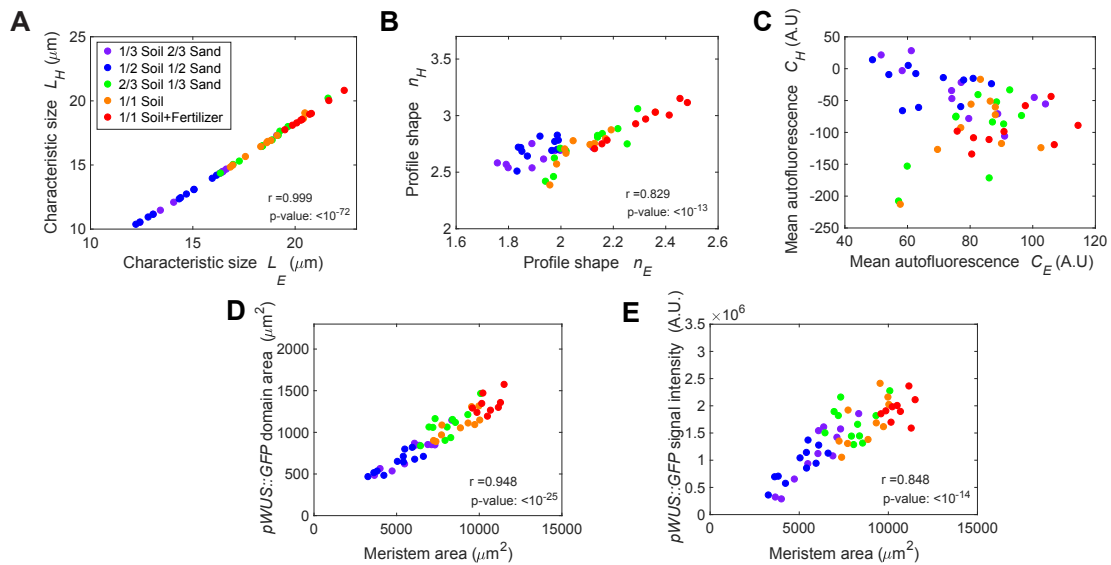


Figure 3.- Quantitative analysis of expression domains in the inflorescence meristem. (A-C) Comparison of some of the extracted features using generalised exponential and Hill fits of *pWUS::GFP-ER* fluorescence domains at the inflorescence meristem of plants growing in different conditions (see [12] for further details): (A) characteristic sizes L_E and L_H , (B) profile parameters n_E and n_H and (C) inferred mean autofluorescence C_E and C_H . Note that L_E and L_H characteristic sizes, and n_E and n_H

shape parameters show a strong correlation. The mean autofluorescence inferred by the Hill fitting C_H exhibits negative values, which shows that the Hill fitting is not optimal for the $pWUS::GFP-ER$ fluorescence profiles. (D-E) Study of how meristem size relates to the $pWUS::GFP-ER$ expression domain at the inflorescence meristem, using the features from the generalised exponential fit. Both $pWUS::GFP-ER$ domain size and total intensity correlate very well with the inflorescence meristem size at different growth conditions. Meristem size has been manually computed as in [12]. Domain area is computed assuming it spans a circular region of radius L_E . The legend found within panel A applies to all panels. At the bottom of panels A-B and D-E, the Pearson linear correlation coefficient r and its p-value are specified. Dataset extracted from [12, 16].

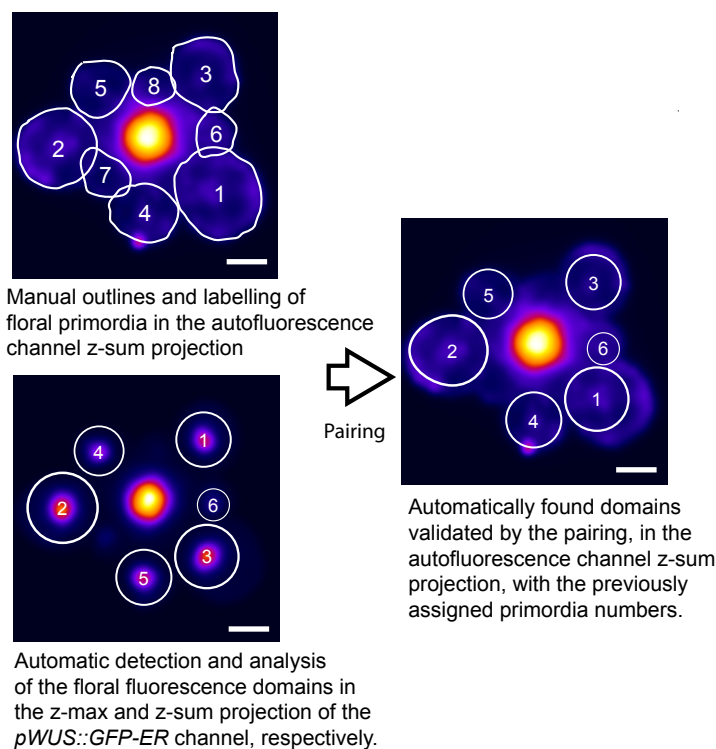


Figure 4.- Sketch of the floral meristems pipeline. Pre-processing steps similar than in Fig. 2 have been omitted for simplicity. The core of the pipeline is the automatic

detection and analysis of the floral fluorescence domains. The manual outline and the pairing of the manual and automatic analysis offers the possibility to extract more information, and for instance, facilitates the study of the phyllotactic pattern; to illustrate it, in the manually outlined floral primordia, the meristems have been manually labelled by order of appearance. Scale bars: 50 μm .

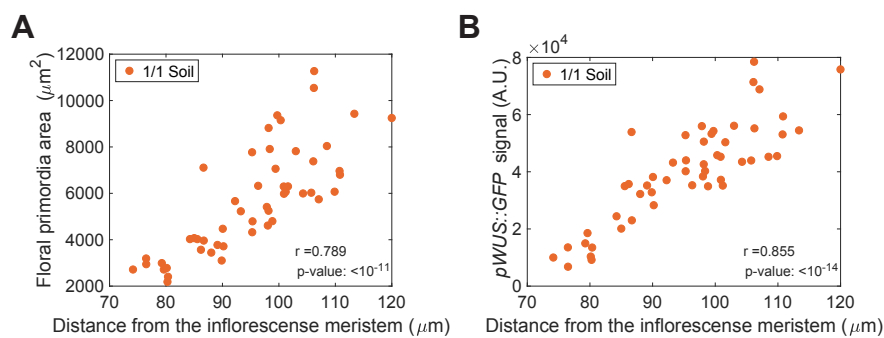


Figure 5.- Quantitative analysis of floral meristems and expression domains. (A)

Floral meristem projected area increases with the distance to the centre of the inflorescence meristem. The distances have been computed from the centroids of the automatically detected *pWUS::GFP-ER* floral domains to the centroid of the automatically detected *pWUS::GFP-ER* inflorescence domain. Note that this plot is possible thanks to pairing the outlines of the floral primordia, which enables to compute the areas, and the automatically found fluorescence domains. (B) Study of the correlation between floral meristem distance to the centre of the inflorescence domain and the total signal of the *pWUS::GFP-ER* marker. The total signal has been computed by subtracting the autofluorescence extracted from the generalised exponential fit. In each panel, the Pearson coefficient r and its p-value are specified.

Dataset extracted from [12, 16].